Molecular Crystals and Liquid Crystals
Publication details, including instructions for authors and subscription information:
http://www.tandfonline.com/loi/gmcl16

A Study of Flow Alignment Instability During Rectilinear Oscillatory Shear of Nematics

M. G. Clark [a] , F. C. Saunders [a] , I. A. Shanks [a] & F. M. Leslie [b]
[a] Royal Signals and Radar Establishment, Malvern, Worcs., WR14 3PS, U.K.
[b] Mathematics Department, University of Strathclyde, Glascow, G1 1XH, U.K.
Version of record first published: 14 Oct 2011.

To cite this article: M. G. Clark , F. C. Saunders , I. A. Shanks & F. M. Leslie (1981): A Study of Flow Alignment Instability During Rectilinear Oscillatory Shear of Nematics, Molecular Crystals and Liquid Crystals, 70:1, 195-222

To link to this article: http://dx.doi.org/10.1080/00268948108073590

Mol. Cryst. Liq. Cryst., 1981, Vol. 70, pp. 195–222
0026-8941/81/7001-0195 $06.50/0

Printed in the United States of America

A Study of Flow Alignment Instability During Rectilinear Oscillatory Shear of Nematics†

M. G. CLARK, F. C. SAUNDERS and I. A. SHANKS

Royal Signals and Radar Establishment, Malvern, Worcs. WR14 3PS, U.K.

and

F. M. LESLIE

Mathematics Department, University of Strathclyde, Glascow G1 1XH, U.K.

(*Received September 4, 1980*)

Rectilinear oscillatory shearing of nematic liquid crystals in thin large-area (10 cm × 8 cm × 10 μm) cells has been studied in the range 20 to 100 Hz for two uniform initial alignments, one planar and parallel to the direction of oscillation and the other homeotropic. In the former case, for certain positive values of the viscosity coefficient α_3 a flow-alignment instability occurs above a critical amplitude A_c for the displacement of the movable upper plate, leading to formation of regular cm-wide bands of alternating 2π and -2π twist, running parallel to the alignment direction. The width of the bands decreases with decreasing temperature and increasing frequency, the total number present depending on the size of the cell. In homeotropic alignment, similar bands of lower twist form at an angle to the direction of oscillation, in this case both for certain positive values of α_3 and, in addition, for α_3 slightly negative. A theoretical expression for A_c in the cases with $\alpha_3 > 0$ has been derived and substantially confirmed experimentally. The theory further predicts the existence of a remarkable "stability gap" where, although the expression for A_c is a minimum, there is no instability and formation of bands should not occur. By exploiting the divergence of α_3 at a smectic A phase, theory and experiment have been compared over a wide range of α_3 values, and the stability gap confirmed experimentally for several materials. In the case of "weak" smectic phases (i.e., showing actual or incipient re-entrant behavior) the expected divergence of A_c does not occur until significantly inside the smectic phase range. Extrapolation of $1/A_c^2$ against temperature can be used to locate accurately the temperature at which α_3 is zero. A variety of materials has been studied, revealing that α_3 may be positive in a rather wider range of

† Presented at the Eighth International Liquid Crystal Conference, Kyoto, Japan, June 30–July 4, 1980.

materials than had previously been realized, and that when α_3 is positive it usually remains so over most or all of the nematic range.

1 INTRODUCTION

It is well known that the flow properties of a nematic liquid are characterized by six coefficients denoted α_1 to α_6, of which two in particular, α_2 and α_3, describe the coupling between flow and director orientation.[1] There are important qualitative and quantitative differences between the flow properties of materials with $\alpha_3 < 0$ and those with $\alpha_3 > 0$: when subjected to steady simple shear flow, materials in the first class align with their director at a fixed angle to the velocity ("flow alignment") for all magnitudes of shear, whereas materials with $\alpha_3 > 0$ do not. Both classes of material may show hydrodynamic instabilities when subjected to suitable shear flows. Previous workers have studied instabilities induced by constant or very low frequency (less than a few Hz) shear for both rectilinear[2-7] and couette flow[8, 9] and by high (ultrasonic) frequency rectilinear shear.[10, 11] Both Pieranski, Guyon, and coworkers[2-7] and Cladis and Torza[8, 9] have identified instabilities associated with $\alpha_3 > 0$. More recently, Skarp *et al.*[12, 13] have studied the behavior of a material with $\alpha_3 > 0$ under the shear induced by relative rotation of two discs.

In this paper we report experimental and theoretical studies of a new and unusual hydrodynamic instability induced by rectilinear oscillatory shearing of thin nematic films at frequencies in the range 20–100 Hz. Motivated by a need to understand the hydrodynamics of nematics as part of our work on advanced liquid crystal displays, we have concentrated particularly on the behavior of homogeneously aligned films sheared parallel to the alignment direction. In such cells the instability occurs only if $\alpha_3 > 0$, when it takes the form of centimeter-wide spatially-periodic bands (visible between crossed polars) parallel to the alignment direction. Even more remarkably, we predict and observe that in the region where one might expect the smallest critical amplitude of shearing for instability, the motion is in fact stable and bands do not occur. The behavior of homeotropically-aligned cells, although broadly similar, differs in detail with formation of bands occurring both for $\alpha_3 > 0$ and when α_3 is slightly negative. We have observed these effects in a wide variety of materials (Table I), and it is clear from our work that α_3 may be positive in a rather wider range of materials than was perhaps realized previously, including materials that do not actually show a smectic phase.

In Section 2 of this paper our experimental procedures are detailed and the experimental observations broadly outlined. A necessarily rather approximate, theoretical calculation of the motions leading to the instability is given in Section 3, and used for a detailed discussion and interpretation of our results in Section 4.

TABLE I

Summary of materials considered in this paper

Denotation	Composition (wt % / formulae)	Phase transitions (°C)	Temperature at which $\alpha_3 = 0$ (°C)*
K21	$C_7H_{15}\cdot C_6H_4\cdot C_6H_4\cdot CN$	K30N42.8 I	31(S)
K24	$C_8H_{17}\cdot C_6H_4\cdot C_6H_4\cdot CN$	K21.5S_A33.5N40.5 I	38(C)
80KMT	80% K21 11% M24 ($C_8H_{17}O\cdot C_6H_4\cdot C_6H_4\cdot CN$) 9% T15 ($C_5H_{11}\cdot C_6H_4\cdot C_6H_4\cdot C_6H_4\cdot CN$)	N61.2 I	48.5(S)
79KMT	79% K21 12% M24 9% T15	N60.6 I	48.5(S)
75KMT	75% K21 16% M24 9% T15	N12 S_A20 N62 I	31(S)
ZLI 518	Proprietary mixture of esters (E Merck)	N80 I	73(S)
ZLI 1085	Proprietary mixture of esters (E Merck)	K0N83 I	[88] (S)
SSM	$R.C_6H_{10}\cdot CO_2\cdot C_6H_4\cdot OR'$ 42% R = C_5H_{11} R' = C_8H_{17} 40% R = C_5H_{11} R' = C_5H_{11} 18% R = C_5H_{11} R' = C_3H_7	S_A28N 76.6 I	[≥80] (S)

*S = shear cell method C = conoscopic method.
[ ] denotes temperature greater than clearing point.

2 EXPERIMENTS

2.1 Apparatus and procedures

The cells used were constructed from glass plates approximately 10 cm by 8 cm in area; 3 mm thick glass was used to ensure adequate rigidity. The inner surfaces of both plates were treated either with PVA rubbed parallel to the intended direction of oscillation to produce low tilt homogeneous alignment parallel to the applied velocity, or with lecithin to produce homeotropic alignment with the director perpendicular to the plates. The plates were spaced, normally at 10 μm, by inserting short (2–3 mm) lengths of glass fiber, which also served as rollers so that the top plate moved freely with respect to the bottom one. The overall thickness variations across empty cells, determined by counting interference fringes for sodium light, was typically 2–3 μm.

A fiducial mark on the upper glass surface enabled the amplitude of oscillation during shearing to be measured. Cells were capillary filled and the alignment was then checked between crossed polarizers to ensure its uniformity.

Figure 1 shows the apparatus used to apply shear. The equilibrium temperature of the enclosure was controlled to within $\pm 0.5°$C in the range 5°C to 90°C by use of a P.I.D. temperature controller driving two resistive heating bars with, in addition, cold nitrogen gas circulated into the enclosure when cooling below room temperature. A settling time of 15–30 min. was normally allowed between selected temperatures to ensure that the cell was in equilibrium with the enclosure.

The bottom plate of the cell was secured to the apparatus, and the top plate attached *via* a rigid linkage to a linear actuator driven from a signal generator whose amplitude and frequency could be varied. Observation confirmed that the linear actuator was fully capable of driving the upper plate, with the fiducial mark moving smoothly and appearing to follow the waveform produced by the signal generator precisely.

The cell was viewed in transmission through glass windows in the enclosure. Illumination was provided by a variable-rate xenon strobe lamp, and polarized and analyzed by use of high-quality polaroid. Visual examinations were normally made with the analyzer crossed. The peak-to-peak amplitude of oscillation of the upper plate was measured by setting the strobe frequency to match the frequency of oscillation, thus visually slowing down the motion, and determining the extremities of movement of the fiducial mark with the travelling microscope. Data on the width of the bands was obtained by arranging for the travelling microscope to rack across the cell. Measurements of the amplitude of oscillation and the widths are accurate to about 0.001 cm.

We have also made determinations of the sign of α_3 by the conoscopic

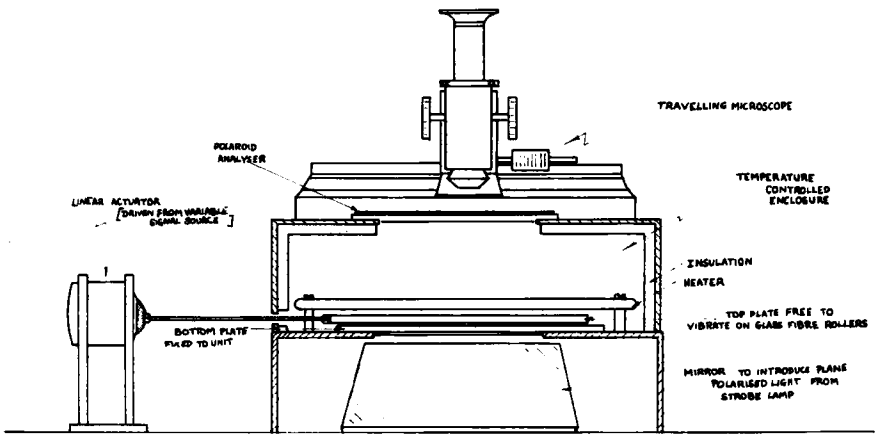

FIGURE 1 Apparatus used for oscillatory rectilinear shearing of nematic films.

method of Pieranski and Guyon.[3] Cells were made from 7 cm by 2 cm microscope slides, with zero tilt homogeneous alignment produced by 30° evaporation of silicon monoxide, and spaced with 100 μm ballotini. The conoscopic figure was obtained for filtered mercury light. We formed the impression that the amount of shearing of the upper plate required to displace the conoscopic figure correlates with the magnitude of α_3 for both signs of α_3. We experienced some difficulty in achieving satisfactory control of the temperature of the sample because of the short working distance between objective and sample required for conoscopy, and the necessity to administer carefully controlled displacements of the upper plate of the cell. A glass heater plate using a transparent tin oxide resistive heating element was inserted under the cell, and the equilibrium temperatures on the upper and lower surfaces of the cell were measured. Inevitably this procedure gave a small temperature gradient of about 1–2° C across the cell, the arithmetic mean being taken as the sample temperature. For several materials in which α_3 changes sign within the nematic range, it was possible to find a temperature range 2–3° C wide within which the conoscopic figure would not move when sheared, with α_3 positive below this range and negative above it. The inversion temperatures T_0 determined in this way agreed with the more accurate values obtained from shear cell data as described in Section 4. Since with the conoscopic apparatus it was easier to perform a controlled increase in temperature than a decrease, conoscopic determination of T_0 tended, if anything, to give a slightly higher temperature corresponding to α_3 becoming observably negative.

2.2 Outline of observations

2.2.1 Homogeneously aligned nematics with $\alpha_3 > 0$ Observations have been made on all the materials listed in Table I. Viewed between crossed polars the homogeneously aligned sample initially appears uniformly dark. On applying a small oscillation of the upper plate of the shear cell, some materials (e.g. ZLI 518, ZLI 1085, SSM) remain dark while above some well-defined frequency-independent amplitude of oscillation others (e.g. the KMT mixtures) show slight color changes as the director apparently tilts and twists out of the alignment direction. The critical amplitude of this homogeneous instability is continuous through the smectic phase of 75KMT. Homogeneous instabilities have been observed in the studies of very low frequency and constant shears cited in Section 1.

In either case, as the amplitude is increased further, we find (excepting certain situations discussed below) an instability leading to regular spatially-periodic large-scale bands parallel to the direction of shear. As shown in Figure 2, the bands always extend across the full width of the cell, but do not necessarily occupy its total length [e.g., Figure 2 (b)]. The light colored (pink or blue with our lamp) bands are separated by thin dark lines. Although with

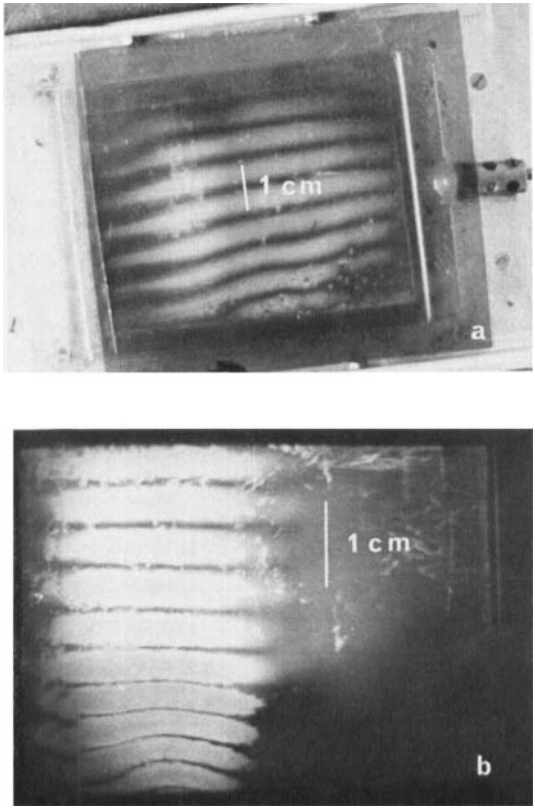

FIGURE 2 Photographs of bands produced by oscillatory shearing of homogeneously aligned, nominally 10 μm, films of ZLI 518 (see Table I) at room temperature, viewed through crossed polarizers: a) A case in which the bands completely fill the cell (frequency of oscillation = 50 Hz). b) A case in which bands fill only half the cell (frequency of oscillation = 100 Hz).

experience pre-transitional distortions of the motion can be clearly identified, the onset of well-formed bands is quite sharp, and the critical amplitude can be measured reproducibly as a function of temperature and frequency. The width of the bands decreases with increasing frequency, but increases with increasing temperature or thickness of cell, and is independent of the amplitude of oscillation. The transmitted light appears to be approximately circularly polarized in opposite senses for alternate bands, suggesting loss of guiding within the liquid crystal due to a relatively tightly twisted structure. In Section 4.3 we argue that the well-formed bands consist of alternating regions of 2π and -2π twist separated by thin (dark) lines of zero twist. Analysis of the motion by strobing indicates that the band structure, once formed, is quite stable while the oscillatory shear is maintained, and does not try to relax back to the homogeneous state during each cycle even at the low repetition rate of 20 Hz.

If the amplitude of oscillation is further increased, an instability consisting of small-scale rolls with diameters comparable with the cell thickness can be observed, using the microscope, in the central region of each light band. The axes of these "mechanical Williams domains" are perpendicular to the oscillation direction. On increasing the amplitude even more, "dynamic scattering", giving a frosty appearance to the naked eye, appears with a well-defined boundary across the cell. Instabilities having these small-scale structures are well known for liquid crystals, and indeed are rather more obviously to be expected than the large-scale band structure.

2.2.2 Homogeneously aligned nematics with $\alpha_3 < 0$ Observations have been made on K15 (n-$C_5H_{11} \cdot C_6H_4 \cdot C_6H_4 \cdot CN$), MBBA (n-$C_4H_9 \cdot C_6H_4 \cdot N{:}CH \cdot C_6H_4 \cdot OCH_3$), and K21 in the region where it has $\alpha_3 < 0$. Application of a small oscillatory shear tends to give a slight uniform color change, viewing with crossed polarizers, presumably as the material adopts some modulated flow alignment tilt. On increasing the amplitude, no large-scale band-structure instability is ever observed, although the mechanical dynamic scattering described in Section 2.2.1 occurs at high amplitude.

2.2.3 Homeotropically aligned nematics with $\alpha_3 > 0$ Observations have been made on ZLI 518. Shearing above a critical amplitude produces spatially-periodic bands similar in dimensions and appearance, viewed between crossed polarizers, to the homogeneous case, but running at an angle of 35°-40° to the direction of oscillation [Figure 3(a)]. Both possible orientations may sometimes be seen simultaneously in different areas of the same cell.

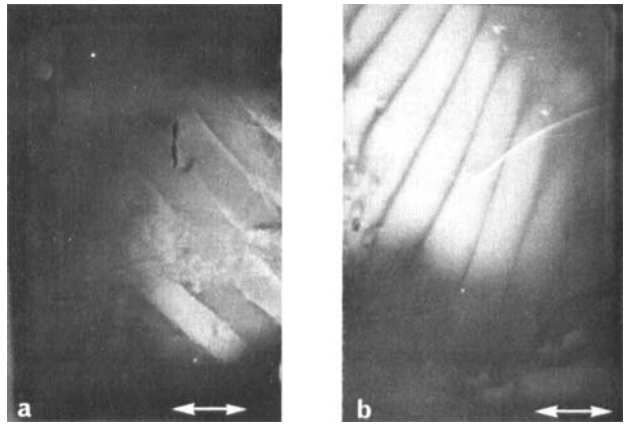

FIGURE 3 a) Photograph of bands produced by oscillatory shearing at 100 Hz of a homeotropically aligned 10 μm film of ZLI 518 at room temperature, viewed through crossed polarizers. b) Photograph of bands produced by oscillatory shearing at 100 Hz of a homeotropically aligned 10 μm film at K15 at room temperature, viewed through crossed polarizers. In both cases the direction of oscillation is shown with double-headed arrows.

The transmitted light appears to be almost linearly polarized in the same direction (parallel to the direction of oscillation) as the incident light, indicating that the structure is different and less twisted than the homogeneous case. Analysis of the motion by strobing indicates that even in well-formed bands the director is relaxing back towards the homeotropic state on each cycle.

Mechanical dynamic scattering can be observed at high amplitudes.

2.2.4 Homeotropically aligned nematics with $\alpha_3 < 0$ Observations were made on K15. A small shear apparently tilts the material homogeneously along the direction of oscillation. However, above a critical amplitude, bands remarkably similar to those found for homeotropically aligned ZLI 518 are obtained [Figure 3(b)]. Again, bands at both orientations to the direction of oscillation have been observed, and on strobing the motion the director is seen to relax back towards the homeotropic state on each cycle.

Mechanical dynamic scattering is again seen at high amplitudes.

3 THEORY

In this Section we present a first attempt at analyzing the flow phenomena leading to the large-scale band structures described above. We consider here only the flow up to and infinitesimally beyond threshold, thus obtaining a description of the critical amplitude and initial growth of the instability, but not addressing the question of what determines the spatial periodicity of the bands that are finally observed.

Intuition, supported by more detailed calculations,[14] suggests that the limiting case of infinitely large periodicity gives a reasonably accurate prediction of the onset of the instability. Further, we treat the instability as primarily a flow phenomenon, thus setting the Frank elastic coefficients equal to zero and neglecting the consequent influences of surface alignment. This can be justified by consideration of the Ericksen number[15, 16] for the problem:

$$\mathrm{Er} = \frac{\text{viscous stress}}{\text{elastic stress}} = \frac{\mu d^2 u'}{K} = \frac{\mu d \omega A}{K} \cos\omega t = \mathrm{Er}^0 \cos\omega t \qquad (3.1)$$

where d is the thickness of the nematic film, μ and K are appropriate viscous and elastic coefficients, and the velocity gradient across the film u' has been approximated by

$$u' = \left(\frac{\omega A}{d}\right) \cos\,\omega t, \qquad (3.2)$$

$A \sin \omega t$ being the displacement of the upper plate of the cell. In our problem normally $\mathrm{Er}^0 \sim 10^2$. Since the fraction of the cell thickness taken up by bound-

ary layers influenced by the surface alignment is[1] $(Er^0)^{-1/2}$ we might expect errors of order 10% due to this approximation. As to the influence of elastic constants on the bulk flow, we may be reassured that the Ericksen number remains high as we enter the instability, since we see a long-period structure of disclination-free bands separated by walls, in contrast with the mass of disclinations reported for couette and viscometric flows.[9, 16] The subsequent appearance of mechanical Williams domains and dynamic scattering at higher shears could be associated with the tendency to limit the rise in Ericksen number by forming regions of high elastic energy as suggested by White *et al.*[16] However, the estimation of Er^0 does merit greater care as a smectic A phase is approached, since the coefficients K_{22}, K_{33}, α_1, α_3, and α_6 diverge.[17] For homogeneous and homeotropic alignments one could argue that the appropriate elastic and viscous coefficients are K_{11}, η_2, and K_{33}, η_1 respectively, where we define the Miesowicz viscosities by

$$\begin{aligned} \eta_1 &= \tfrac{1}{2}(-\alpha_2 + \alpha_4 + \alpha_5) \\ \eta_2 &= \tfrac{1}{2}(\alpha_3 + \alpha_4 + \alpha_6) \\ \eta_3 &= \tfrac{1}{2}\alpha_4 \end{aligned} \tag{3.3}$$

Thus, as we approach a smectic phase, whereas in homogeneous alignment we might predict $Er^0 \to \infty$, in the case of homeotropic alignment $Er^0 \to 0$ and our approach would be suspect. Finally, as in our previous calculations,[18] we neglect all inertial terms for the reasons advanced by Pieranski *et al.*[19]

With the above assumptions, the continuum hydrodynamic equations[20, 21] become, in Cartesian tensor notation,

$$v_{i,i} = 0, \quad n_i n_i = 1, \tag{3.4}$$

$$t_{ij,j} = p_{,i}, \quad g_i = \gamma n_i, \tag{3.5}$$

where **v** is the velocity, **n** the director, p the pressure modified to account for gravity, and γ is an arbitrary scalar. The stress tensor **t** and the intrinsic body torque **g** take the forms

$$t_{ij} = \alpha_1 A_{kp} n_k n_p n_i n_j + \alpha_2 N_i n_j + \alpha_3 N_j n_i + \alpha_4 A_{ij} + \alpha_5 A_{ik} n_k n_j + \alpha_6 A_{jk} n_k n_i, \tag{3.6}$$

$$g_i = -\gamma_1 N_i - \gamma_2 A_{ik} n_k \tag{3.7}$$

where

$$2A_{ij} = v_{i,j} + v_{j,i}, \quad 2N_i = 2\dot{n}_i - (v_{i,j} - v_{j,i})n_j \tag{3.8}$$

and

$$\gamma_1 = \alpha_3 - \alpha_2, \quad \gamma_2 = \alpha_6 - \alpha_5 = \alpha_3 + \alpha_2 \tag{3.9}$$

using the Parodi[22] relation.

3.1 Homogeneous alignment

Taking the z axis perpendicular to the nematic film and the x axis parallel to the displacement of the upper plate, $\mathbf{v}$, $\mathbf{n}$, and p have the forms

$$v_x = u(z, t),\ v_y = v(z, t),\ v_z = 0 \tag{3.10}$$

$$n_x = \cos\theta(z, t)\cos\phi(z, t),\ n_y = \cos\theta(z, t)\sin\phi(z, t),$$
$$n_z = \sin\theta(z, t) \tag{3.11}$$

$$p = p(z, t) \tag{3.12}$$

where t denotes time. Clearly, our choice immediately satisfies the constraints (3.4). Also, the first of Eq. (3.5) has a solution in which

$$t_{xz} = X(t), \quad t_{yz} = Y(t), \tag{3.13}$$

$X(t)$ and $Y(t)$ being arbitrary functions of time. The second of Eq. (3.5) combined with (3.7) and (3.9) yields, after elimination of the scalar γ,

$$\gamma_1\dot{\theta} + K(\theta)(u'\cos\phi + v'\sin\phi) = 0 \tag{3.14}$$

$$\gamma_1\cos^2\theta\dot{\phi} - L(\theta)(u'\sin\phi - v'\cos\phi) = 0 \tag{3.15}$$

where

$$K(\theta) = \alpha_3\cos^2\theta - \alpha_2\sin^2\theta,\ L(\theta) = \alpha_2\sin\theta\cos\theta, \tag{3.16}$$

and the prime and dot denote partial differentiation with respect to z and t, respectively. Employing (3.6), the expressions (3.13) lead to equations for the velocity gradients

$$(M(\theta) + N(\theta))(u'\cos\phi + v'\sin\phi) + K(\theta)\dot{\theta}$$
$$= X(t)\cos\phi + Y(t)\sin\phi \tag{3.17}$$

$$M(\theta)(u'\sin\phi - v'\cos\phi) - L(\theta)\dot{\phi} = X(t)\sin\phi - Y(t)\cos\phi \tag{3.18}$$

where

$$2M(\theta) = \alpha_4 + (\alpha_5 - \alpha_2)\sin^2\theta,\ 2N(\theta)$$
$$= (\alpha_3 + \alpha_6 + 2\alpha_1\sin^2\theta)\cos^2\theta \tag{3.19}$$

By elimination of the flow gradients, (3.14) and (3.15) could be reduced to a pair of equations for θ and ϕ in terms of the applied tractions. However, for our purpose it is more convenient to combine (3.14) and (3.17) to yield

$$G(\theta)(u'\cos\phi + v'\sin\phi) = X(t)\cos\phi + Y(t)\sin\phi \tag{3.20}$$

$$\gamma_1 G(\theta)\dot{\theta} + K(\theta)(X(t)\cos\phi + Y(t)\sin\phi) = 0 \tag{3.21}$$

with

$$\gamma_1 G(\theta) = \gamma_1(M(\theta) + N(\theta)) - K^2(\theta). \tag{3.22}$$

Similarly, (3.15) and (3.18) yield

$$H(\theta)(u' \sin \phi - v' \cos \phi) = X(t) \sin \phi - Y(t) \cos \phi \tag{3.23}$$

$$\gamma_1 \cos^2 \theta H(\theta)\, \dot{\phi} = L(\theta)(X(t) \sin \phi - Y(t) \cos \phi) \tag{3.24}$$

where

$$\gamma_1 \cos^2 \theta H(\theta) = \gamma_1 \cos^2 \theta M(\theta) - L^2(\theta) \tag{3.25}$$

and the viscosity functions $G(\theta)$ and $H(\theta)$ are both always positive.[23]

For motions with **n** and **v** confined to the xz plane, (3.20) and (3.21) reduce to

$$G(\theta)u' = X(t), \quad \gamma_1 G(\theta)\dot{\theta} + K(\theta)X(t) = 0 \tag{3.26}$$

while (3.23) and (3.24) are automatically satisfied provided that there is no transverse component of stress. Taking (3.2) for the velocity gradient, equations (3.26) combine to yield

$$\dot{\theta} = -(\sin^2 \theta + \epsilon \cos^2 \theta) B\omega \cos \omega t \tag{3.27}$$

where

$$\epsilon = -\frac{\alpha_3}{\alpha_2}, \quad B = \frac{|\alpha_2| A}{\gamma_1 d} \tag{3.28}$$

assuming that α_2 is always negative. Integration of (3.27) yields

$$\tan \theta = \begin{cases} -\epsilon^{1/2} \tan\left[\left(\frac{A}{d}\right)(\epsilon^{-1/2} + \epsilon^{1/2})^{-1} \sin \omega t\right] & \epsilon > 0 \quad (3.29) \\ |\epsilon|^{1/2} \tanh\left[\left(\frac{A}{d}\right)(|\epsilon|^{-1/2} - |\epsilon|^{1/2})^{-1} \sin \omega t\right] & \epsilon < 0 \quad (3.30) \end{cases}$$

choosing $\theta = 0$ at $t = 0$ in both cases.

When $\alpha_3 < 0$, the oscillations in the tilt angle θ are bounded for all A, these bounds never exceeding the flow alignment angles, $\pm \arctan(|\epsilon|^{1/2})$, for constant shear. However, when $\alpha_3 > 0$, although the oscillations of θ are small if both ϵ and A are small, the amplitude of oscillation increases quite rapidly as A increases, with $\tan \theta$ diverging for a critical amplitude

$$A_c = \tfrac{1}{2}\pi d(\epsilon^{-1/2} + \epsilon^{1/2}) \tag{3.31}$$

In order to investigate the stability of the in-plane motion we consider small

perturbations from the plane of the imposed shear, and seek to determine when such deviations will grow in magnitude. Thus if the angle ϕ and the transverse flow component v are non-zero but small, one again obtains (3.26) from (3.20) and (3.21), but (3.23) and (3.24) now yield

$$H(\theta)(u'\phi - v') = X(t)\phi, \quad \gamma_1 \cos^2\theta H(\theta)\dot{\phi} = L(\theta)X(t)\phi, \tag{3.32}$$

this assuming that the transverse component of shear stress is negligible. Combining the second members of (3.26) and (3.32) we obtain

$$\frac{d\phi}{d\theta} = \frac{\tan\theta G(\theta)\phi}{H(\theta)(\sin^2\theta + \epsilon\cos^2\theta)} \tag{3.33}$$

Rewriting the functions $G(\theta)$ and $H(\theta)$ defined by (3.22) and (3.25) in the simpler forms

$$G(\theta) = \eta(1 + 2\beta\sin^2\theta\cos^2\theta), \quad H(\theta) = \eta(\sin^2\theta + \lambda\cos^2\theta) \tag{3.34}$$

where

$$\eta = \eta_1 - \alpha_2^2/\gamma_1, \quad 2\eta\beta = (\gamma_2^2/\gamma_1) + \alpha_1, \quad \eta\lambda = \eta_3, \tag{3.35}$$

both η and λ being necessarily positive,[23] and making the substitution

$$s = \tan^2\theta \tag{3.36}$$

then (3.33) becomes

$$\frac{2d\phi}{\phi ds} = \frac{s^2 + 2(1+\beta)s + 1}{(s+1)(s+\lambda)(s+\epsilon)} \tag{3.37}$$

In the general case $1 \neq \epsilon \neq \lambda \neq 1$ this yields

$$\frac{\phi^2}{\phi_0^2} = (1 + \tan^2\theta)^a(1 + \epsilon^{-1}\tan^2\theta)^b(1 + \lambda^{-1}\tan^2\theta)^c \tag{3.38}$$

where ϕ_0 is the value of ϕ at $\theta = 0$ and

$$a = \frac{2\beta}{(1-\epsilon)(\lambda-1)}, \; b = \frac{(1-\epsilon)^2 - 2\beta\epsilon}{(1-\epsilon)(\lambda-\epsilon)}, \; c = \frac{(1-\lambda)^2 - 2\beta\lambda}{(1-\lambda)(\epsilon-\lambda)} \tag{3.39}$$

Note that $a + b + c = 1$. Various special cases follow either directly from (3.37) or by taking appropriate limits of (3.38):

if $1 = \epsilon \neq \lambda$

$$\frac{\phi^2}{\phi_0^2} = (1 + \tan^2\theta)^k(1 + \lambda^{-1}\tan^2\theta)^{1-k}\exp\left[\frac{2\beta\sin^2\theta}{(1-\lambda)}\right] \tag{3.40}$$

$$k = \frac{2\beta\lambda}{(1-\lambda)^2}$$

if $l = \lambda \neq \epsilon$

$$\frac{\phi^2}{\phi_0^2} = (1 + \tan^2\theta)^l (1 + \epsilon^{-1}\tan^2\theta)^{1-l} \exp\left[\frac{2\beta \sin^2\theta}{(1-\epsilon)}\right] \tag{3.41}$$

$$l = \frac{2\beta\epsilon}{(1-\epsilon)^2}$$

if $\epsilon = \lambda \neq 1$

$$\frac{\phi^2}{\phi_0^2} = (1 + \tan^2\theta)^{-m}(1 + \epsilon^{-1}\tan^2\theta)^{1+m} \exp\left\{\frac{[(1-\epsilon)^2 - 2\beta\epsilon]\tan^2\theta}{\epsilon(1-\epsilon)(\epsilon + \tan^2\theta)}\right\} \tag{3.42}$$

$$m = \frac{2\beta}{(1-\epsilon)^2}$$

if $1 = \epsilon = \lambda$

$$\frac{\phi^2}{\phi_0^2} = \sec^2\theta \exp[\beta \sin^4\theta] \tag{3.43}$$

We suppose that for a flow alignment instability to occur, two conditions must be satisfied. First, when the amplitude A becomes sufficiently large the ratio $n_y^2/(n_y^0)^2$, where n_y^0 is the y component of the director for $\theta = 0$, must attain either very large or very small values during the motion. The former case corresponds to small transverse perturbations, when the director is in the plane of the cell, being amplified when the director turns out of the plane, and the latter to transverse perturbations, when it is out of the plane, becoming amplified as it returns to the plane. Second, large deviations in θ must occur during the motion, since the finite amplitude instability is driven by the intrinsic non-linearity arising from the θ-dependence of the coefficients in the equations of motion.

Since the thermodynamic inequality $\gamma_1 > 0$ implies that $\epsilon > -1$, it is evident from (3.30) that the second condition is not satisfied when $\alpha_3 < 0$. Clearly this is not so when $\alpha_3 > 0$, and to investigate the first condition we examine the quantity

$$Z = \frac{(n_y^2)_{\theta=\pi/2}}{(n_y^2)_{\theta=0}} = \lim_{\theta \to \pi/2} \cos^2\theta\left(\frac{\phi^2}{\phi_0^2}\right) \tag{3.44}$$

It is convenient to distinguish the three regions $\epsilon \ll 1$, $\epsilon \sim 1$, and $\epsilon \gg 1$. Thus, when $\epsilon \ll 1$, (3.38) gives

$$Z \approx \epsilon^{-1/\lambda}\lambda^{-c} \gg 1 \qquad (1 \neq \lambda \neq \epsilon) \tag{3.45}$$

while the special cases (3.41) and (3.42) yield

$$Z \approx \epsilon^{-1} e^{2\beta} \gg 1 \qquad (\lambda = 1) \tag{3.46}$$

and

$$Z \approx \epsilon^{-1-2\beta} \exp\left[\frac{1}{\epsilon}\right] \gg 1 \qquad (\lambda = \epsilon) \tag{3.47}$$

Evidently the instability is expected when $0 < \epsilon \ll 1$.

However, if $\epsilon \sim 1$, (3.40) and (3.43) yield

$$Z \approx \lambda^{-1+k} \exp\left[\frac{2\beta}{(1-\lambda)}\right] \qquad (\lambda \neq \epsilon) \tag{3.48}$$

and

$$Z \approx e^{\beta} \qquad (\lambda = \epsilon) \tag{3.49}$$

respectively. In this case Z is 0(1) and, although the expression for the critical amplitude A_c is a minimum, the planar motion is expected to be stable.

Finally, when $\epsilon \gg 1$, (3.38), (3.41), and (3.42) yield

$$Z \approx \epsilon^{(2\beta/\epsilon)-1} \lambda^{2\beta\lambda/\epsilon(1-\lambda)} \qquad (1 \neq \lambda \neq \epsilon) \tag{3.50}$$

$$Z \approx \epsilon^{(2\beta/\epsilon)-1} \exp\left[-\frac{2\beta}{\epsilon}\right] \qquad (1 = \lambda \neq \epsilon) \tag{3.51}$$

$$Z \approx \epsilon^{-1} \exp\left[\frac{2\beta}{\epsilon} - 1\right] \qquad (\lambda = \epsilon) \tag{3.52}$$

where

$$\frac{2\beta}{\epsilon} \approx \frac{|\alpha_2|}{\eta_1}\left(\frac{\alpha_1}{\alpha_3} + 1\right) \tag{3.53}$$

noting that since $\epsilon \gg 1$ is associated with pre-smectic behavior, α_1 will also be large in magnitude. The case $\lambda = \epsilon$, (3.52), is not expected in practice since λ does not diverge at a nematic to smectic phase transition. Thus our analysis predicts that an instability with $Z \gg 1$ will occur provided $2\beta > \epsilon$. If $2\beta < \epsilon$ an instability with $Z \ll 1$ is predicted. In either case it could be argued that the threshold may become less marked as $\epsilon \to \infty$, since the factor $\epsilon^{1/2}$ premultiplying tan in (3.29) will cause θ to be large even before A attains A_c. However, we have seen no direct evidence for this, although we would not exclude the possibility that such a large premultiplier could be one of the factors involved in the homogeneous color change transition mentioned in Section 2.2.1.

3.2 Homeotropic alignment

Retaining the Cartesian axes used in Section 3.1, we now take spherical coor-

dinates with the azimuth θ measured relative to the yz plane. Thus

$$n_x = \sin\theta,\ n_y = \cos\theta\sin\phi,\ n_z = \cos\theta\cos\phi \tag{3.54}$$

By mathematical analysis rather similar to that detailed in Section 3.1 we obtain for the basic planar motion

$$\tan\theta = \begin{cases} \epsilon^{-1/2}\tan\left[\left(\frac{A}{d}\right)(\epsilon^{-1/2}+\epsilon^{1/2})^{-1}\sin\omega t\right] & \epsilon > 0 \quad (3.55) \\ |\epsilon|^{-1/2}\tanh\left[\left(\frac{A}{d}\right)(|\epsilon|^{-1/2}-|\epsilon|^{1/2})^{-1}\sin\omega t\right] & \epsilon < 0 \quad (3.56) \end{cases}$$

When $\alpha_3 > 0$, the oscillations of θ are again unbounded, with $\tan\theta$ diverging when $\sin\omega t = 1$ for a critical amplitude A_c given by the same formula, (3.31), as in homogeneous alignment. Examination of small perturbations from the plane of the imposed shear yields

$$\frac{\phi^2}{\phi_0^2} = (1+\tan^2\theta)^a(1+\epsilon\tan^2\theta)^b(1+\lambda\tan^2\theta)^c \tag{3.57}$$

[where a, b, and c are given by (3.39)] for the general case $1 \neq \epsilon \neq \lambda \neq 1$, with special cases analogous to (3.40)–(3.43). The three cases $\epsilon \ll 1$, $\epsilon \sim 1$, and $\epsilon \gg 1$ can be discussed with similar results to homogeneous alignment, except that $1/Z$ is large or small according as Z would have been large or small in homogeneous alignment. Thus (except when $1 \ll \epsilon > 2\beta$) the instability is associated with $Z \ll 1$. This means that small perturbations when the director is in the plane of the cell will be amplified when it returns to a perpendicular orientation; actually the same mechanism as that operated for homogeneous alignment. However, arguments above concerning the Ericksen number cast doubt on the neglect of elasticity effects when $\epsilon \gtrsim 1$ in homeotropic alignment. Thus, our principal result is that a flow alignment instability should occur if $0 < \epsilon \ll 1$, with the same critical amplitude as in homogeneous alignment. One could argue that the threshold might become less marked as $\epsilon \to 0$ because of the factor $\epsilon^{-1/2}$ premultiplying tan in (3.55), although we have not observed evidence of this in practice.

If $\alpha_3 < 0$, the oscillations of θ are bounded, never exceeding $\pm$ arccot $(|\epsilon|^{1/2})$. This corresponds to tilt angles lying between $\pi/2$ and the flow alignment angle. The factor $|\epsilon|^{-1/2}$ premultiplying tanh in (3.56) means that, in contrast to homogeneous alignment, large deviations in θ can occur during the motion if $|\epsilon|$ is small. Further, from (3.57) and (3.39)

$$Z \propto (1-|\epsilon|\tan^2\theta)^{1/\lambda} \tag{3.58}$$

can become very small as $\tan^2\theta \to 1/|\epsilon|$. Thus we predict, and observe, a flow

alignment instability for small negative α_3, in contrast with homogeneous alignment. Since (3.56) shows no obvious divergent feature, an expression for the critical amplitude in this case appears to be beyond the scope of the present calculation. However, we show in Section 4 that the observed critical amplitudes correspond to θ attaining a fixed, large, value, supporting our basic assumption that the strong non-linearities associated with large amplitude oscillations of θ are an essential requirement for the instability.

4 DISCUSSION AND INTERPRETATION

4.1 Materials with $\epsilon > 0$

We consider first the region $0 < \epsilon \ll 1$. Figure 4 shows plots of A_c against temperature for both homogeneously and homeotropically aligned 10 μm

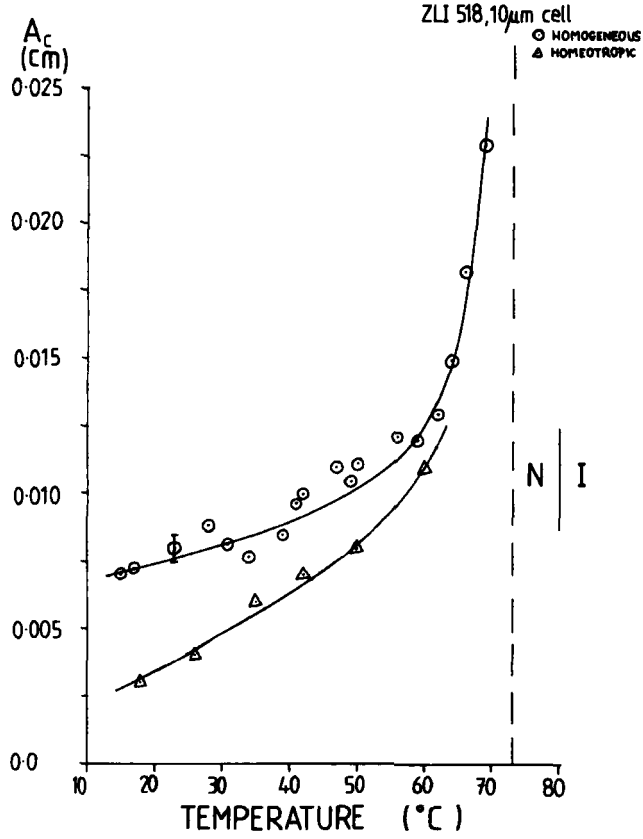

FIGURE 4 Plots of critical amplitude A_c against temperature for both homogeneously and homeotropically aligned 10 μm cells containing ZLI 518. The broken line shows the temperature at which $\alpha_3 = 0$.

cells containing ZLI 518. In this material ϵ is small and positive at room temperature and decreases to zero with increasing temperature. The difference in critical amplitude of the two cells is significant only at lower temperatures where the Ericksen number is smaller. The prediction that the critical amplitude is independent of frequency is very well confirmed by all our data, even in regions where some effects due to lower Ericksen number are perceptible. Table II gives some sample data. An attempt was also made to verify that $A_c \propto d$, but unfortunately the only glass fibers available to us with diameters other than 10μm were not very satisfactory as cell spacers with the result that we were able to confirm this result only qualitatively.

The inversion temperature at which $\epsilon = 0$ can be located accurately by supposing that close to its zero ϵ is a linear function of temperature. Then, by (3.31), $1/A_c^2$ should be a linear function of temperature. Figure 5 confirms that $1/A_c^2$ does indeed give linear extrapolations for the data in Figure 4, thus supporting the $\epsilon^{-1/2}$ dependence of A_c predicted by (3.31). Further, the data for homogeneous and homeotropic cells extrapolate to exactly the same temperature (73° C). The agreement here will be aided by the fact that the temperature at which $1/A_c^2$ vanishes is independent of cell thickness and by the increasing Ericksen number. We believe that extrapolation in this way is an accurate and convenient method for determining the inversion temperature; a similar extrapolation was used by Pieranski, Guyon, and Pikin[5] in their studies of a different instability in HBAB (4-n-hexyloxybenzilidene-4'-aminobenzonitrile).

A further advantage of the $1/A_c^2$ extrapolation procedure is illustrated by the data for ZLI 1085 summarized in Figure 6. This material has a rather similar temperature variation of ϵ, except that the extrapolation shows clearly that the inversion temperature is above the clearing point. Conoscopic examination confirms that $\alpha_3 > 0$ up to the clearing point, but cannot, of course, give a value for the "virtual" inversion temperature. The ester mixture denoted SSM in Table I also has a virtual inversion temperature. Indeed, it is our gen-

TABLE II

Sample of data taken for ZLI 518 in a 10 μm homogeneously aligned cell, illustrating the frequency independence of A_c

	Values of A_c, in cm, at various temperatures			
Freq./Hz	17°C	34°C	41°C	50°C
10	0.008			
20	0.008	0.008	0.010	0.011
30	0.008	0.008	0.009	0.011
40	0.008	0.008	0.010	0.011
50	0.007	0.007	0.009	0.012
60	0.006	0.008	0.010	0.011
70	0.006	0.007	0.010	0.011

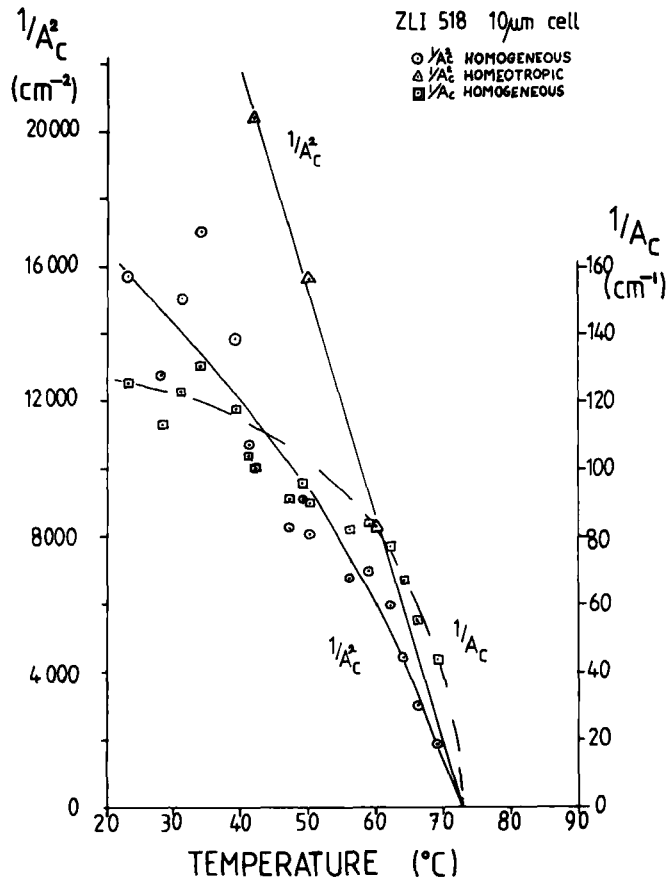

FIGURE 5 Plots of $1/A_1$ and $1/A_1^2$ against temperature for data taken from Figure 4. Note that $1/A_1^2$ extrapolates linearly to the temperature at which $\alpha_3 = 0$.

eral observation that if α_3 is positive over part of the nematic range of a material it tends to be positive over much or all of that range.

Figure 7 shows data on the width of the bands in a 10 μm homogeneous cell containing ZLI 518, plotted as the number of bands per unit length as a function of frequency of oscillation and temperature. The number of bands observed in a cell is the integer nearest the ratio of the active width of the cell divided by the width W of the bands, suggesting an analogy with convective instabilities. Notice that the data extrapolate to $W \sim 1$ cm at zero frequency, corresponding for our cells to rather more bands than for the anticipated lowest mode of one or two bands per cell. The natural scaling laws of the variables[24] suggest that d/W should be a function of $df^{1/2}$, where f is the frequency of oscillation, but it is evident from our data that this function is certainly not

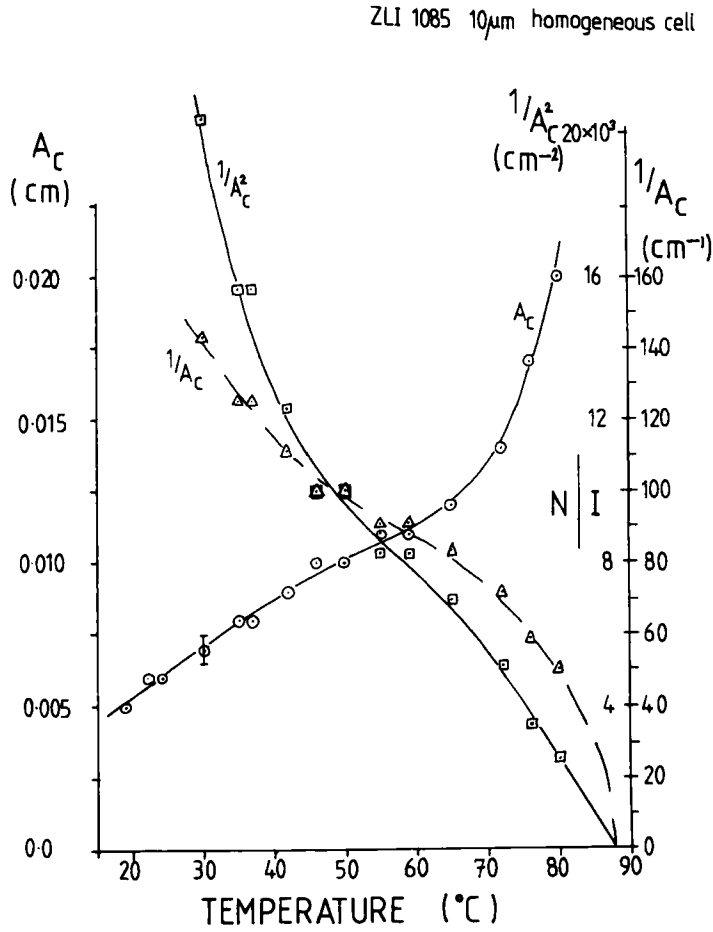

FIGURE 6 Plots of A_c, $1/A_c$, and $1/A_c^2$ against temperature for ZLI 1085 in a 10 μm homogeneously-aligned cell. Note that $\alpha_3 \to 0$ at a "virtual" inversion temperature above the clearing point.

linear. If we further suppose that the function requires a dimensionless argument, the simplest form is

$$\left(\frac{\mu d^2 f}{K}\right)^{1/2} = (\tau_d f)^{1/2} \tag{4.1}$$

where μ and K are appropriate viscosity and elasticity coefficients and τ_d is a free relaxation time. Thus

$$\frac{d}{W} = F(\tau_d f) \tag{4.2}$$

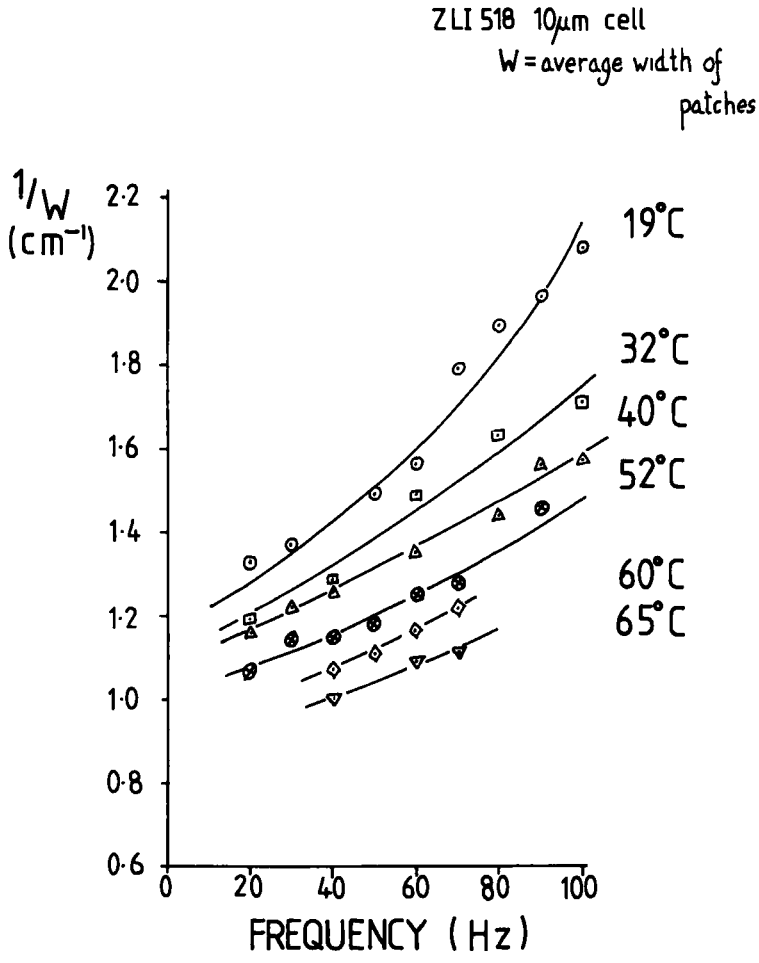

FIGURE 7 Data on the average width of the bands in a 10 μm homogeneously-aligned cell containing ZLI 518, plotted as the number of bands per unit length, $1/W$, against frequency of oscillation for various temperatures. The width is independent of the amplitude of oscillation to within experimental error.

where, from Figure 7, the function F increases as its argument increases. Eq. (4.2) implies that W should increase with increasing temperature (since τ_d surely decreases) and with increasing d, both of which are confirmed by our experiments.

We turn now to the region of larger positive ϵ. To explore this region we have studied several materials showing actual or incipient smectic behavior. Figure 8 shows a plot of A_c against temperature for a Demus ester mixture denoted SSM in a 10 μm homogeneous cell. As temperature is decreased from the virtual inversion temperature of 80°C or more, ϵ increases, attaining the

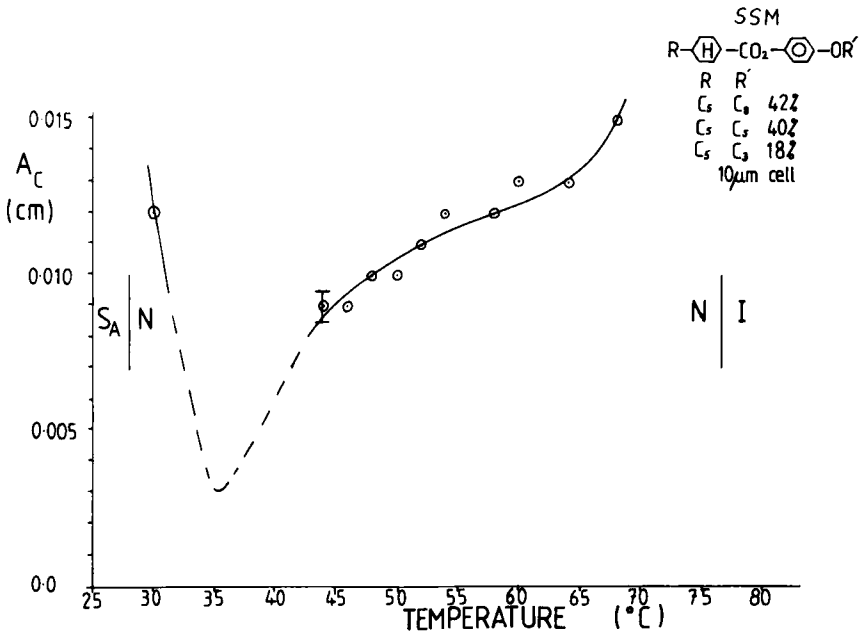

FIGURE 8 Plot of A_c against temperature for the Demus ester mixture denoted SSM in a 10 μm homogeneous cell. The solid curves show the temperature regions in which it was possible to observe bands, and the broken curve the "stability gap."

value unity at about 35° C and diverging to $+\infty$ as the temperature approaches the nematic to smectic A phase transition at 28° C. The solid line in Figure 8 shows temperature regions in which it was possible to observe bands, with points identifying temperatures at which careful measurements of A_c were made. In agreement with theoretical predictions, we observe a "stability gap" around the minimum in A_c. The curve in this region has been interpolated using the theoretical value πd for the minimum of A_c. Notice that the divergence of A_c, and ϵ, occurs significantly outside the "strong" smectic phase shown by this material.

The influence of incipient and actual smectic A phases can be explored by use of mixtures showing re-entrant behavior. Figure 9 shows data taken in 10 μm homogeneous cells for three re-entrant mixtures based on cyanobiphenyl materials.[25] As the ratio of K21 to M24 is reduced we pass from an incipient smectic phase to an actual phase with a central temperature of 16° C. Thus the mixture with 80% K21, denoted 80KMT, shows a steady increase in ϵ as the temperature is lowered from the inversion temperature of 48.5° C, but the incipient smecticity is insufficient for ϵ to approach unity even close to the central temperature of 16° C. However, a slight decrease in the K21:M24 ratio to 79% K21, although insufficient to cause the smectic phase to occur, is suffi-

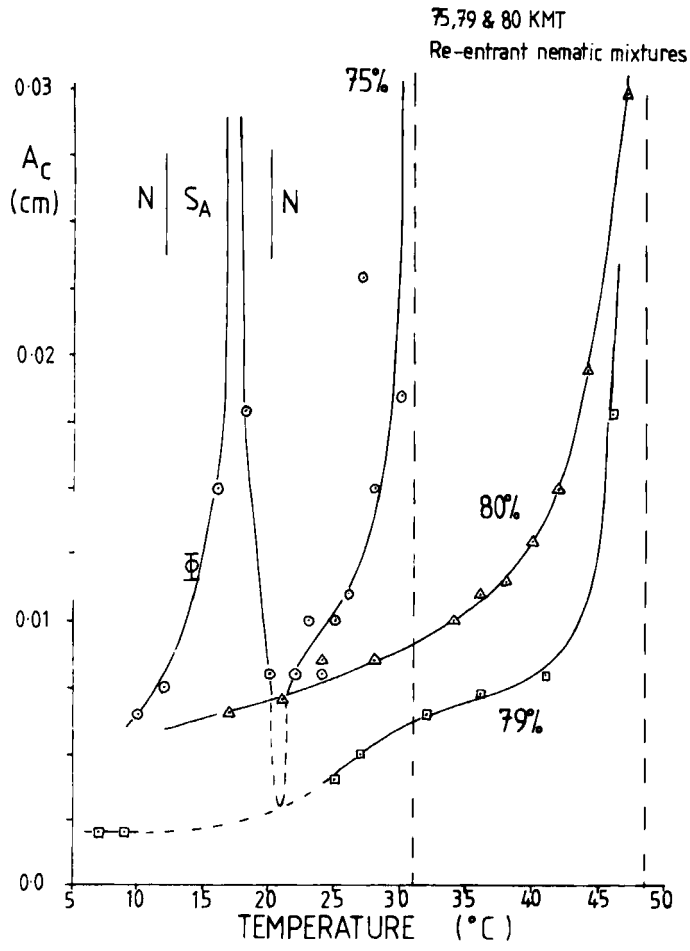

FIGURE 9 Plots of A_c against temperature for the mixtures 75KMT, 79KMT, and 80KMT of cyanobiphenyl and cyanoterphenyl materials in 10 μm homogeneous cells. The vertical broken lines show temperatures at which $\alpha_3 = 0$ for the respective mixtures and the broken curves stability gaps. The N-S_A-N phase boundaries shown apply to 75KMT.

cient for its influence to raise ϵ to about unity in the region of the central temperature, causing a stability gap. The values of A_c below the stability gap are unexpectedly low for reasons which are not yet clear but appear not to include experimental error.

Further decrease in the K21:M24 ratio to 75% K21 causes a smectic A phase to appear in the range 16 ± 4°C. Unfortunately the inversion temperature (but not the clearing point) is sharply lowered to 31°C so that the variation of ϵ in the upper nematic range, from zero at 31°C to divergence to $+\infty$ on entering the smectic phase, is rather rapid. On leaving the smectic phase to the lower

nematic, a rapid decrease in ϵ from $+\infty$ is observed. Notice that the divergence of A_c due to this "weak" smectic phase does not occur until the temperature is significantly inside the smectic region. The phase transition temperatures observed in the actual cell used agreed well with separate microscopical observations. Further, in the absence of shear, the alignment of the smectic, as judged by use of polaroid and the unaided eye, appeared uniform homogeneous even after the cell had been subjected to prolonged and vigorous oscillatory shearing within the smectic range. Perhaps the effect could be interpreted in terms of suppression of the transition to the smectic phase by the imposed shear (cf. de Gennes[26]).

Figure 10 shows the plots of $1/A_c^2$ against temperature used to determine the inversion temperatures; notice the particularly good linear extrapolation for 80KMT.

Data on two individual cyanobiphenyl compounds, studied in 10 μm homogeneous cells, are shown in Figure 11. The upper panel shows a plot of critical amplitude against temperature for K21. The material was supercooled without difficulty and we were able to observe ϵ increasing from zero at 31°C as the temperature was decreased. The observation of positive α_3 below 31°C, which was confirmed by the conoscopic method, suggests that the observations of Skarp *et al.*[27] on K21, using a Wahl-Fischer rotational shear flow apparatus, may perhaps require reinterpretation taking into account neglected factors such as the radial shear gradient and elastic forces.

The lower panel in Figure 11 shows the critical amplitude for K24. The data are very similar to those for the upper nematic range of 75KMT, with rapid variation in ϵ and penetration of the instability into the (by inference) "weak" smectic phase. Skarp *et al.*[13] have reported measurements of ϵ for K24 obtained by use of a Wahl-Fischer apparatus in which an electric field could be applied across the nematic film. The values of ϵ extracted from the data shown in Figure 11 by use of (3.31) are in poor agreement with theirs, but it must be remembered that for our values, at least, the estimated errors are quite large ($\pm 30\%$), due mainly to uncertainty in the precise value of d, and that we estimate above that factors neglected in our theory were of the order of 10%. Skarp *et al.* have also reported[12] that when the rotational shear imposed by relative rotation of the circular plates of the Wahl-Fischer apparatus is large enough they observe dark concentric bands. These bands differ from those reported here in several respects: they are observed without use of an analyzer, they remain for some time after rotation has stopped (whereas our bands disappear immediately shearing is stopped), and the ratio of band width to cell thickness W/d is smaller in their case at roughly 10 compared with 10^3. We suggest that their bands may involve formation of disclinations, possibly in substantial numbers, in a manner analogous to that observed by Cladis and Torza[9] in couette flow. The observations of Hiltrop and Fischer[28] on radial Poiseuille flow may also be relevant.

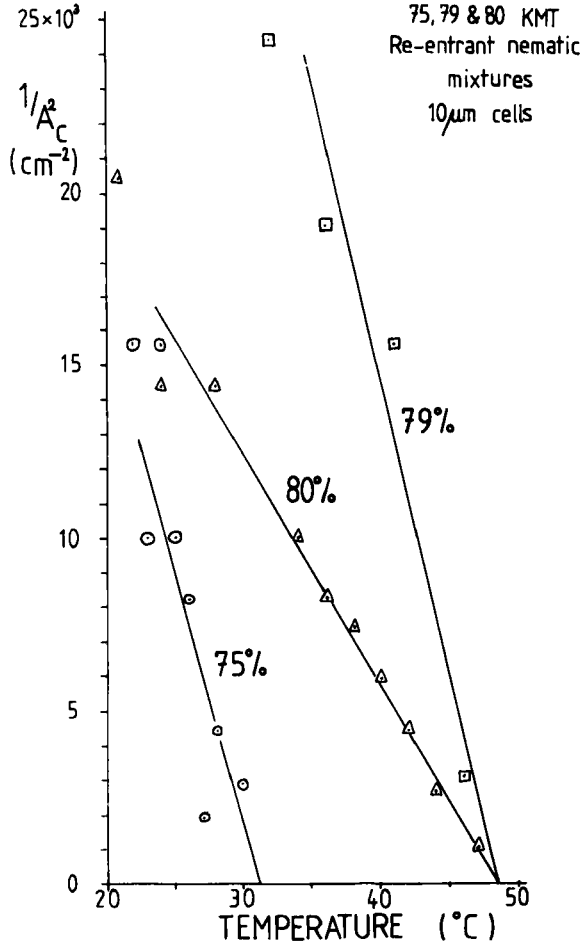

FIGURE 10 Extrapolations of $1/A_c^2$ against temperature for data taken from Figure 9.

4.2 Materials with $\epsilon < 0$

As noted above, if $\epsilon < 0$ flow alignment instability leading to large W/d bands is observed only for homeotropic alignment. Table III gives data on the critical amplitude A_c for observation of these bands in K15. The last column in the table gives the corresponding values of the amplitude θ_c of the oscillations of θ, calculated using measurements of ϵ taken from Skarp *et al.*[27] It is seen that over a fourfold change in A_c the critical amplitude θ_c is constant within experimental error. Thus it seems that the instability occurs when the amplitude of the planar motion reaches about 73.5°, supporting the arguments given in Section 3.2.

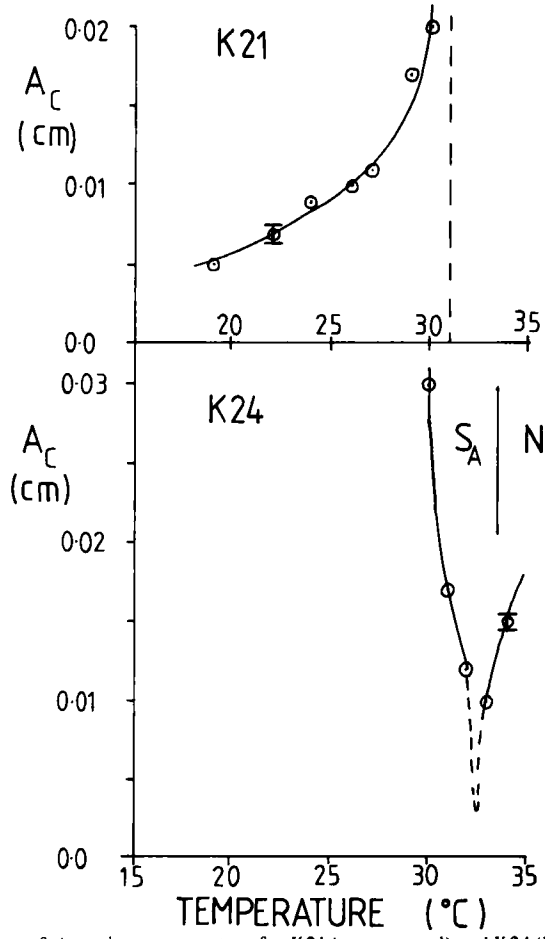

FIGURE 11 Plots of A_c against temperature for K21 (upper panel) and K24 (lower panel) in 10 μm homogeneous cells. Broken vertical line in upper panel shows inversion temperature of K21, and broken curve in lower panel shows inferred stability gap for the shearing of K24.

TABLE III

Critical amplitude and director azimuth as a function of temperature for K15 in a homeotropically aligned 10 μm cell

Temperature/°C	Critical amplitude A_c/cm	θ_c[a]
18	0.002	[63.1°]
20	0.003	70.1°
25	0.004	73.4°
29	0.006	75.7°
33	0.008	74.9°

[a] θ_c values are calculated from Eq. (3.56) using values of ϵ taken from Skarp *et al.*;[27] [ ] signifies that ϵ was obtained by extrapolation outside the temperature range for which data were reported.

4.3 Structure of the bands

The bands observed in homogeneous and homeotropic cells are rather similar in that they have large W/d ratios of order 10^3, and frequency independent critical amplitudes A_c which are approximately the same for both alignments if $\alpha_3 > 0$. These similarities are consistent with our theory in which the infinitesimal instability is broadly similar in all cases in which bands occur. However, as outlined in Section 2, the bands differ in structure reflecting differences in the finite instabilities. These differences may be qualitatively understood by considering the different topological constraints imposed by the two alignments.

It is convenient to represent the variation of the director through the cell by the locus traced out on the unit sphere by the tip of the vector $\mathbf{n}(z)$ as z varies from zero to d. The locus is drawn in two dimensions as its stereographic projection on the equatorial plane of the sphere. Analogous representations were used by Van Doorn[29] and Berreman.[30]

Referring to Figure 12, when $A = 0$ the locus for homogeneous alignment is a point on the equatorial plane (or, strictly, tilted above 2° above it for rubbed PVA alignment). As A increases, the amplitude at one extreme of the planar motion is a double line running up towards the pole of the sphere. The

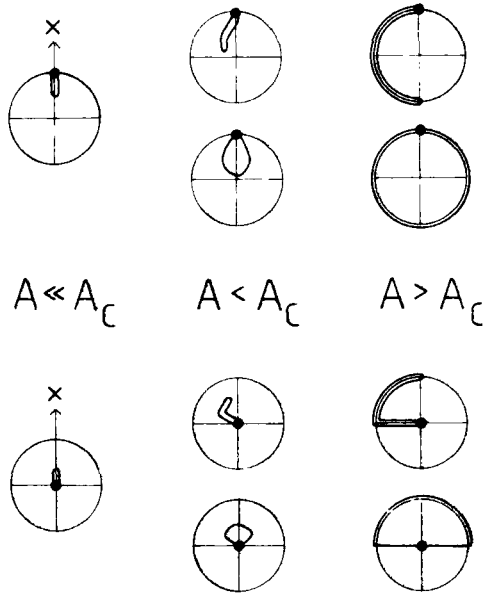

FIGURE 12 Upper part shows stereographic projections of possible director configurations at one extreme of the motion during oscillatory shearing of thin homogeneously-aligned nematic films. Lower part shows the corresponding diagrams for homeotropically-aligned films. In both cases some lines have been separated slightly for clarity. The heavy dot shows the configuration in the absence of shear, and the direction of the applied oscillation is parallel to x.

effect of deviations out of the plane as the director becomes upright might be to deflect this line or open it into a loop at its upper end. In the limit, the former leads to $\pi + (-\pi)$ twist and the latter to 2π twist. It is difficult to distinguish these two possibilities by their optical transmission without elaborate measurements. However, the stroboscopic observations (Section 2.2.1) favor the 2π structure since this appears significantly more inhibited from relaxing back to the homogeneous state than the $\pi + (-\pi)$ structure. Thus, as noted in Section 2.2.1, the observed structure is interpreted as alternate 2π and -2π bands separated by walls of zero twist. The topology of such walls has been discussed by Stieb and Labes.[31]

With prolonged shearing above the critical amplitude it is possible to form small irregular patches apparently having an odd twist, probably $\pm\pi$. These patches are separated from the main $\pm 2\pi$ twist by narrow walls or disclinations, and whereas the $\pm 2\pi$ bands disappear the instant shearing is stopped, the patches, as might be expected, disappear completely only after a short period of time. The odd and even twists are also distinguished by the orientation of mechanical Williams domains. In both cases the rolls form perpendicular to the direction of **n** at the center of the layer. Thus they are perpendicular to the direction of oscillation for the $\pm 2\pi$ bands and parallel to it for the $\pm\pi$ patches.

Returning to Figure 12, in the case of homeotropic alignment the locus when $A = 0$ is a point at the pole. As A increases the locus of the amplitude at one extreme of the motion becomes a double line running down towards the equator. Deviations out of the plane can again either displace this line or form a loop, leading in the limit to $\frac{1}{2}\pi + (-\frac{1}{2}\pi)$ or π twisted structures, respectively. It is not obvious that these possibilities can be distinguished on the available experimental evidence. Neither appears particularly inhibited against relaxation to the homeotropic configuration, consistently with stroboscopic observations (Section 2.2.3 and 2.2.4). It is tempting to associate the slightly lower critical amplitudes observed for homeotropic alignment (Figure 4) with the lower elastic energy of the less twisted structures formed. The significance of the non-zero angle between the bands and the direction of oscillation in homeotropic alignment is unclear; any slight ellipticity in the motion of the upper plate could obviously be a factor.

Since the period of the applied shear in our experiments is always shorter than the free relaxation time for director re-orientation, the appearance of relatively high twists in the observed flow alignment instabilities could be rationalized in terms of selection of a faster-responding mode as the steady state solution left after transients have died away.

Acknowledgments

We thank D. G. McDonnell, R. A. Smith, and E. P. Raynes for assistance with experimental mixtures, P. A. Holland and C. T. Smith for helping with the construction of apparatus, and K. Skarp

and colleagues for preprints and discussion concerning their work. F. M. L. gratefully acknowledges support by the Procurement Executive, U. K. Ministry of Defense.

References

1. P. G. de Gennes, *The Physics of Liquid Crystals*, (Clarendon Press, Oxford, 1974), Chap. 5.
2. P. Pieranski and E. Guyon, *Phys. Rev.*, **A9**, 404 (1974).
3. P. Pieranski and E. Guyon, *Phys. Rev. Lett.*, **32**, 924 (1974).
4. P. Pieranski and E. Guyon, *Commun. Phys.*, **1**, 45 (1976).
5. P. Pieranski, E. Guyon, and S. A. Pikin, *J. Phys.* (*Paris*) *Colloq.*, **37**, C1 3 (1976).
6. P. Manneville and E. Dubois-Violette, *J. Phys.* (*Paris*), **37**, 285 (1976); **37**, 1115 (1976).
7. M. Cohen, P. Pieranski, E. Guyon, and C. D. Mitescu, *Mol. Cryst. Liq. Cryst.*, **38**, 97 (1977).
8. P. E. Cladis and S. Torza, *Phys. Rev. Lett.*, **35**, 1283 (1975).
9. P. E. Cladis and S. Torza, *Colloid Interface Sci.*, **4**, 487 (1976).
10. F. Scudieri, *Appl. Phys. Lett.*, **29**, 398 (1976).
11. K. Miyano and Y. R. Shen, *Appl. Phys. Lett.*, **28**, 473 (1976).
12. K. Skarp, T. Carlsson, I. Dahl, S. T. Lagerwall, and B. Stebler, Proc. 3rd Liq. Cryst. Conf. Soc. Countries (Budapest, 1979).
13. K. Skarp, T. Carlsson, S. T. Lagerwall, and B. Stebler, 8th Internat. Liq. Cryst. Conf. (Kyoto, 1980), paper C-2P.
14. M. G. Clark and F. M. Leslie, unpublished work.
15. E. Guyon and P. Pieranski, *J. Phys.* (*Paris*) *Colloq.*, **36**, C1 203 (1975).
16. A. E. White, P. E. Cladis, and S. Torza, *Mol. Cryst. Liq. Cryst.*, **43**, 13 (1977).
17. F. Jähnig and F. Brochard, *J. Phys.* (*Paris*), **35**, 301 (1974).
18. M. G. Clark and F. M. Leslie, *Proc. Roy. Soc. Lond.*, **A361**, 463 (1978).
19. P. Pieranski, F. Brochard, and E. Guyon, *J. Phys.* (*Paris*), **34**, 35 (1973).
20. J. L. Ericksen, *Trans. Soc. Rheol.*, **5**, 23 (1961).
21. F. M. Leslie, *Arch. Rat. Mech. Anal.*, **28**, 265 (1968).
22. O. Parodi, *J. Phys.* (*Paris*), **31**, 581 (1970).
23. F. M. Leslie, *Advanc. Liq. Cryst.*, **4**, 1 (1979).
24. J. L. Ericksen, *Trans. Soc. Rheol.*, **13**, 9 (1969).
25. E. P. Raynes, 7th Internat. Liq. Cryst. Conf. (Bordeaux, 1978), paper EP37.
26. P. G. de Gennes, *Mol. Cryst. Liq. Cryst.*, **34**, 91 (1976).
27. K. Skarp, S. T. Lagerwall, B. Stebler, and D. McQueen, *Phys. Scripta*, **19**, 339 (1979).
28. K. Hiltrop and F. Fischer, *Z. Naturforsch.*, **31a**, 800 (1976).
29. C. Z. Van Doorn, *J. Appl. Phys.*, **46**, 3738 (1975).
30. D. W. Berreman, *J. Appl. Phys.*, **46**, 3746 (1975).
31. A. E. Stieb and M. M. Labes, *Mol. Cryst. Liq. Cryst.*, **45**, 21 (1978).